Article

Multi-Period Fast Robust Optimization for Partial Distributed Generators (DGs) Providing Ancillary Services

Jian Zhang [1], Mingjian Cui [2],* and Yigang He [3],*

1. School of Electrical Engineering and Automation, Hefei University of Technology, Hefei 230009, China; z_jj1219@sina.com
2. Department of Electrical Engineering and Computer Science, The University of Tennessee, Knoxville, TN 37996, USA
3. School of Electrical Engineering and Automation, Wuhan University, Wuhan 430072, China
* Correspondence: mingjian.cui@ieee.org (M.C.); yghe1221@whu.edu.cn (Y.H.)

Abstract: Distributed generators providing auxiliary service are an important means of guaranteeing the safe and economic operation of a distribution system. In this paper, considering an energy storage system (ESS), switchable capacitor reactor (SCR), step voltage regulator (SVR), and a static VAR compensator (SVC), a two-stage multi-period hybrid integer second-order cone programming (SOCP) robust model with partial DGs providing auxiliary service is developed. If the conic relaxation is not exact, a sequential SOCP is formulated using convex–concave procedure (CCP) and cuts, which can be quickly solved. Moreover, the exact solution of the original problem can be recovered. Furthermore, in view of the shortcomings of the large computer storage capacity and slow computational rate for the column and constraint generation (CCG) method, a method direct iteratively solving the master and sub-problem is proposed. Increases to variables and constraints to solve the master problem are not needed. For the sub-problem, only the model of each single time period needs to be solved. Then, their objective function values are accumulated, and the worst scenarios of each time period are concatenated. As an outcome, a large amount of storage memory is saved and the computational efficiency is greatly enhanced. The capability of the proposed method is validated with three simulation cases.

Keywords: ancillary services; CCP; distribution system; robust optimization; sequential SOCP

1. Introduction

In recent years, a large number of DGs and electric vehicles (EVs) have been connected to the distribution network. The intermittence of renewable DGs and EVs aggravates the problem of voltage and current magnitude violation and poor power flow [1]. Further, the interaction between discrete adjustable equipment, DGs and EVs may result in frequent actions of OLTC, SVR, and SCR, speeding up wear and pushing up operation and maintenance costs. In order to cope with the above challenges, the traditional passive distribution network is gradually evolved into an active distribution network. At present, a large number of terminals and communication system have been installed in distribution systems. DGs providing auxiliary services are feasible and great value [2]. However, for a distribution system with a large number of DGs, if all the DGs provide auxiliary services, the total payment from the power company to DG owners will be high. Partial but not all the DGs providing ancillary service are a cost-effective way to ensure the safe and economic operation of a distribution system.

The multi-period programming of active and reactive power is an effective tool to ensure the safe and economic operation of a distribution network [3–5]. Conventionally, the optimal power flow (OPF) problem can be formulated as non-convex nonlinear mixed integer programming. Theoretically, the global optimal solution cannot be sought out in polynomial time. For potential economic benefits, there has been growing interest in

determining the global solution with high computational efficiency. In recent years, many examples of significant progress have been released using convex relaxation methods. Convex relaxation models could be solved more efficiently, and provide a lower bound for the objective value at optimum and may even give the globally optimal solution if the relaxation is exact. The pioneer work in [6] finds that the semi definite programming (SDP) relaxation will be exact for several IEEE benchmark systems after adding a small resistance to every purely inductive transformer branch, and opens up a promising research direction. The geometry of the power flow injection region is investigated in [7,8]. Compared to SDP, the SOCP based on the bus injection model as well as the branch flow model has attracted more attention in radial balanced distribution networks due to its much higher solving efficiency.

Finding a group of sufficient conditions to guarantee exact convex relaxation ex ante is of great value. For the distribution network with radial topology, if the objective function is convex, strictly increasing with line loss, not increasing with load, independent of the active and reactive power flow of lines, then the SOCP relaxation will be exact as long as the original OPF is feasible [9,10]. It is pointed out in [11] that the SOCP relaxation will be exact if (i) the objective function is strictly increasing with active power injection, (ii) there is no reverse power flow, and (iii) there is not an upper limit on voltage amplitude. It is found in [12] that the SOCP relaxation will be exact if there is no simultaneous reversal of active and reactive power flows. Further sufficient conditions on system parameters that can be checked ex ante, which admit a provable exactness guarantee for the overhead line and cable distribution network, are suggested in [13,14], respectively. Although SOCP convex relaxation has been proved to be exact under mild conditions, there are still many factors challenging these conditions in practical applications, especially the influence of objective function. If the objective function is not strictly increasing with node active power injection, then the exactness may not be guaranteed.

The optimization methods of OPF are generally divided into centralized [15] and distributed approaches [16,17]. In [18], the SOCP and SDP models are formulated to solve the multi-period OPF problem of an unbalanced three-phase distribution system with battery ESS. The active and reactive power levels of battery ESS are dispatched to minimize the power losses and energy purchase costs. However, the uncertainty of load and renewable energy is not taken into account.

To address the uncertainty of loads and renewable DGs, two major methods have been widely applied, i.e., stochastic optimization and robust optimization. The robust optimization methods are advantageous for full solution robustness and high computing efficiency. Thus, to guarantee operating robustness against any uncertainty realization, the robust optimization methods are preferred. At present, the CCG robust optimization method is very popular [19,20]. It is widely used to solve the robust optimization problem of a distribution system [21–23]. However, when it is applied to the large-scale multi-period robust optimization of a distribution network, the computational rate is very slow since a huge number of variables and constraints are generated in the master problem. Therefore, it is difficult to meet the requirement of online rolling optimization. In [24], a two-stage robust optimization model of a pre-specified number of photovoltaic (PV) inverters providing ancillary services is developed. Nevertheless, SCR, SVR, SVC and ESS are not taken into account. Further, since the objective function of the model is strict, decreasing with active power injection, when the penetration rate of DGs is high, the conic relaxation could be not exact.

To address the above problem, a sequential convex optimization method to solve broader classes of OPF problems over radial networks is proposed. The nonconvex branch power flow equation is decomposed as a second-order cone inequality and a non-convex constraint involving the difference of two convex functions. Provided with an initial solution offered by an inexact SOCP relaxation, this approach solves a sequence of convexified penalization problems, where concave terms are approximated by linear functions and

updated at each iteration. It could recover a feasible solution, which usually appears to be very close, if not equal, to the global optimal one [25].

According to the literatures review, we find that, in the existing robust optimization with partial DGs providing ancillary services, SCR, SVR, SVC and ESS are not taken into account. Further, the computational rate of CCG is very slow when the distribution system is large and the multi-period model is formulated. Furthermore, when the objective function is not strictly increasing with active power injection and the penetration rate of DGs is high, the conic relaxation could be not exact. In this paper, considering ESS, SCR, SVR, and SVC, a two-stage multi-period hybrid integer SOCP robust model with partial DGs providing auxiliary service is developed. Moreover, the fast solving method is proposed.

Compared with [24], the main contributions of this paper are as follows: (1) The optimization model is extended to multi-period, in which the coordination of ESS, SCR, SVR, and SVC with partial DGs providing ancillary services is formulated. (2) The reactive power of ESS is utilized. (3) The losses of ESS are included in the objective function. (4) If the conic relaxation is not exact, a sequential SOCP is formulated using CCP and cuts, which can significantly improve the convergence rate. (5) Increases to variables and constraints to solve the master problem are not needed. For the sub-problem, only the model of each single time period needs to be solved. Then, their objective function values are accumulated, and the worst scenarios of each time period are concatenated. As an outcome, a large amount of storage memory is saved and the computational efficiency is greatly enhanced. (6) The computing rate of the proposed method is much faster than the CCG method.

The organization of this paper is as follows. In Section 2, considering ESS, SCR, SVR, and SVC, the multi-period robust model for coordinated active and reactive optimization in a distribution network with partial DGs providing ancillary services is formulated. In Section 3, the two-stage mixed integer SOCP and sequential SOCP fast solving method is developed. In Section 4, simulation cases are performed. Concluding remarks are summarized in Section 5.

2. Robust Model for Partial DGs Providing Ancillary Services

2.1. Deterministic Optimization Model

The radial distribution system shown in Figure 1 can be described using branch flow equations. According to [24], considering the ESS, SCR, SVR, and SVC, the multi-period model for active and reactive power coordination with partial DGs providing ancillary services can be formulated as Equations (1)–(18). The models of ESS, SCR, SVC, and SVR are the same as [26], except that the reactive power of ESS shown as Equation (18) is utilized.

Master Problem (MP) :
$$\min_{\{P_{s,j,t},Q_{s,j,t},z_{j,t},u_{j,t},l_{ij,t},H_{ij,t},G_{ij,t},P_{j,t}^{\text{ch}},P_{j,t}^{\text{dis}},P_{j,t}^{\text{ESS}},Q_{j,t}^{\text{ESS}},Q_{j,t}^{\text{SVC}},Q_{j,t}^{\text{SCR}},k_{ij,t}^{\text{SVR}}\}} f_{\text{obj}}$$

$$\sum_{t=1}^{T_{\max}}\left\{\sum_{j\in B^{\text{ESS}}}\left[(1-\eta_{\text{ch}})P_{j,t}^{\text{ch}}+\left(\frac{1}{\eta_{\text{dis}}}-1\right)P_{j,t}^{\text{dis}}\right]+\sum_{(i,j)\in E}r_{ij}l_{ij,t}-\sum_{j\in J}P_{s,j,t}\right\} \quad (1)$$

$$P_{s,j,t}^{f}-P_{L,j,t}-P_{j,t}^{\text{ch}}+P_{j,t}^{\text{dis}}=\sum_{k\in\delta(j)}H_{jk,t}-\sum_{i\in\pi(j)}\left(H_{ij,t}-r_{ij}l_{ij,t}\right),\forall j\in V\backslash J,\forall t \quad (2)$$

$$Q_{j,t}^{\text{ESS}}+Q_{j,t}^{\text{SVC}}+Q_{j,t}^{\text{SCR}}-Q_{L,j,t}=\sum_{k\in\delta(j)}G_{jk,t}-\sum_{i\in\pi(j)}\left(G_{ij,t}-x_{ij}l_{ij,t}\right)+b_{s,j}u_{j,t},\forall j\in V\backslash J,\forall t \quad (3)$$

$$P_{s,j,t}-P_{L,j,t}-P_{j,t}^{\text{ch}}+P_{j,t}^{\text{dis}}=\sum_{k\in\delta(j)}H_{jk,t}-\sum_{i\in\pi(j)}\left(H_{ij,t}-r_{ij}l_{ij,t}\right),\forall j\in J,\forall t \quad (4)$$

$$Q_{s,j,t}+Q_{j,t}^{\text{ESS}}+Q_{j,t}^{\text{SVC}}+Q_{j,t}^{\text{SCR}}-Q_{L,j,t}=\sum_{k\in\delta(j)}G_{jk,t}-\sum_{i\in\pi(j)}\left(G_{ij,t}-x_{ij}l_{ij,t}\right)+b_{s,j}u_{j,t},\forall j\in J,\forall t \quad (5)$$

$$- P_{L,j,t} - P^{\text{ch}}_{j,t} + P^{\text{dis}}_{j,t} = \sum_{k \in \delta(j)} H_{jk,t} - \sum_{i \in \pi(j)} \left(H_{ij,t} - r_{ij} l_{ij,t} \right), \forall j \in B \backslash V, \forall t \tag{6}$$

$$Q^{\text{ESS}}_{j,t} + Q^{\text{SVC}}_{j,t} + Q^{\text{SCR}}_{j,t} - Q_{L,j,t} = \sum_{k \in \delta(j)} G_{jk,t} - \sum_{i \in \pi(j)} \left(G_{ij,t} - x_{ij} l_{ij,t} \right) + b_{s,j} u_{j,t}, \forall j \in B \backslash V, \forall t \tag{7}$$

$$u_{j,t} = u_{i,t} - 2 \left(r_{ij} H_{ij,t} + x_{ij} G_{ij,t} \right) + \left(r_{ij}^2 + x_{ij}^2 \right) l_{ij,t}, \forall (i,j) \in E, \forall t \tag{8}$$

$$\left(U_j^{\min} \right)^2 \le u_{j,t} \le \left(U_j^{\max} \right)^2, \forall j \in B, \forall t \tag{9}$$

$$0 \le l_{ij,t} \le \left(I_{ij}^{\max} \right)^2 \qquad \forall (i,j) \in E, \forall t \tag{10}$$

$$P^f_{s,j,t} (1 - z_{j,t}) \le P_{s,j,t} \le P^f_{s,j,t}, \forall j \in J, \forall t \tag{11}$$

$$\left\| \begin{array}{c} Q_{s,j,t} \\ T_{s,j,t} \end{array} \right\|_2 \le S_j, \forall j \in J, \forall t \tag{12}$$

$$- T_{s,j,t} \tan \theta_j \le Q_{s,j,t} \le T_{s,j,t} \tan \theta_j, \forall j \in J, \forall \theta_j \in \left[0, \frac{\pi}{2} \right), \forall t \tag{13}$$

$$H^2_{ij,t} + G^2_{ij,t} \le l_{ij,t} u_{i,t} \qquad \forall (i,j) \in E, \forall t \tag{14}$$

$$z_{j,t} \in \{0,1\}, \sum_{j \in J} z_{j,t} \le K, \forall j \in J, \forall t \tag{15}$$

$$0 \le T_{s,j,t} \le M z_{j,t}, \forall j \in J, \forall t \tag{16}$$

$$0 \le P_{s,j,t} - T_{s,j,t} \le M z_{j,t}, \forall j \in J, \forall t \tag{17}$$

$$\sqrt{\left(P^{\text{ch}}_{j,t} - P^{\text{dis}}_{j,t} \right)^2 + \left(Q^{\text{ESS}}_{j,t} \right)^2} \le S^{\text{ESS}}_j, \forall j \in B^{\text{ESS}}, \forall t \tag{18}$$

where $P^{\text{ch}}_{j,t}$ and $P^{\text{dis}}_{j,t}$ are the charge and discharge power of ESS at node j time t, respectively. η_{ch} and η_{dis} are the charge and discharge efficiency, respectively. B^{ESS} is the set of nodes connected with ESS. $Q^{\text{ESS}}_{j,t}$ and S^{ESS}_j are the reactive power and rated capacity of ESS. $Q^{\text{SVC}}_{j,t}$ and $Q^{\text{SCR}}_{j,t}$ are the reactive powers of SVC and SCR, respectively. $k^{\text{SVR}}_{ij,t}$ is the turn ratio of SVR between bus i and j, at time t. The term in the objective function $\sum_{j \in B^{\text{ESS}}} \left[(1 - \eta_{\text{ch}}) P^{\text{ch}}_{j,t} + \left(\frac{1}{\eta_{\text{dis}}} - 1 \right) P^{\text{dis}}_{j,t} \right]$ is the total active power losses of ESS. The meanings of other variables and formulas are listed in [24]. They are not explained in any further detail in this paper.
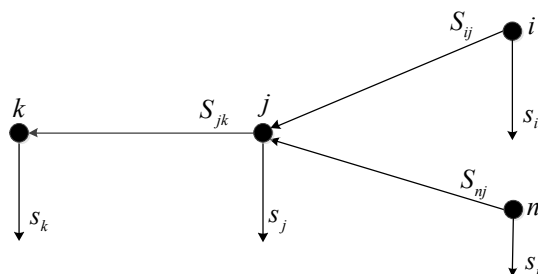
Figure 1. A radial distribution system.

The binaries $z_{j,t}$ and discrete variables associated with SVR and SCR and the discrete as well as continuous variables associated with ESSs are the first-stage variables. Meanwhile, continuous variables such as the reactive power of SVC and branch flows are the second-stage variables. The first-stage variables denoted by $\{\psi_t\}$ cannot be adjusted after the uncertainties are revealed. They are regarded as the "here and after" decisions. The con-

tinuous variables, such as the reactive power of the SVC, branch power, currents, and node voltage magnitudes, are the second-stage variables. The second-stage variables denoted by $\{\varphi_t\}$ can be adaptively changed in the real-time operation when the uncertainties are revealed. Branch power flows, currents, and node voltage magnitudes are also regarded as the state variables, while the reactive power of SVC is the "wait and see" decision.

2.2. Robust Optimization Model

In reality, loads and active power of renewable DGs have strong uncertainty. To hedge against the uncertainty, a robust model is given by

$$\min_{\{\psi_t\}} \quad \max_{\substack{(p_t,q_t) \in D_t \\ P_t^f \in G_t}} \quad \min_{\{\varphi_t\}} f_{\text{obj}} \tag{19}$$

$$\text{s.t. } (1)\sim(18) \tag{20}$$

$$D_t = \left\{ (p_t,q_t) \middle| p_t^{\min} \le p_t \le p_t^{\max}, p_t^{\min} \circ \tan(\theta_L) \le q_t \le p_t^{\max} \circ \tan(\theta_L) \right\} \tag{21}$$

$$G_t = \left\{ P_t^f \middle| P_t^{f\min} \le P_t^f \le P_t^{f\max} \right\} \qquad \forall j \in J \tag{22}$$

In the uncertainty sets, the lower and upper bounds of load and the active power of the DGs $p_t^{\min}$, $p_t^{\max}$, $P_t^{f\min}$, and $P_t^{f\max}$ can be obtained by the interval prediction.

3. Solving Method

3.1. Master Problem

In this paper, a two-stage robust model based on cutting plane is formulated. The master problem is shown in Equations (1)–(18). The objective of the master problem is to find the optimal values of the first-stage variables given the worst scenario generated by the sub-problem. It gives a lower bound of the original problem given by Equations (19)–(22). The optimal values of the first-stage variables, such as $z_{j,t}$, the capacitive admittance of the SCR, the turn ratios of the OLTC and SVR, and the injected power of the ESS, are substituted into Equations (1)–(18). Then, the sub-problem can be formulated.

The master problem shown in Equations (1)–(18) can be written as a compact form as:

$$\text{Master-Problem(MP): } f_{\text{mp}} = \min_{\{\psi_t\},\{\varphi_t\}} f_{\text{obj}} \tag{23}$$

$$\text{s.t. } \psi_t \in \Psi_t \tag{24}$$

$$\sum_{t=1}^{T_{\max}} A_t^T \psi_t \le b \tag{25}$$

$$B_t^T \psi_t \le b_{1t} \tag{26}$$

$$J_t \varphi_t \le b_{2t} \tag{27}$$

$$L_t \psi_t + N_t \varphi_t \le b_{3t} \tag{28}$$

$$D_t^{\text{p}} \psi_t + E_t^{\text{p}} \varphi_t = p_t \tag{29}$$

$$D_t^{\text{q}} \psi_t + E_t^{\text{q}} \varphi_t = q_t \tag{30}$$

$$H_t \varphi_t \le P_{s,t}^f \tag{31}$$

$$\|K_{nt} \varphi_t\|_2 \le h_{nt}^T \varphi_t \tag{32}$$

$$\|C_{nt} \psi_t\|_2 \le O_{nt}^T \psi_t \tag{33}$$

where inequality Equation (32) denotes the conic relaxation of each line and capacity constraints on DGs. Inequality Equation (33) denotes capacity constraints on ESS.

3.2. Sub-Problem

Given the values of the first-stage variables by the master problem, the sub-problem can be written as a compact form as:

$$\text{Sub-Problem (SP): } L\left(\psi_1^*, \cdots \psi_{T_{\max}}^*\right) = \max_{\substack{(p_t, q_t) \in D_t \\ P_t^f \in G_t}} \min \sum_{t=1}^{T_{\max}} \left(c_t^T y_t\right) \tag{34}$$

$$R_t y_t = b_{1t} \forall t, (\pi_{1t}) \tag{35}$$

$$M_t y_t \le b_{2t} \forall t, (\pi_{2t}) \tag{36}$$

$$W_t^{\mathrm{P}} \varphi_t = p_t + p_{0t} \qquad \forall t, (\pi_{3t}) \tag{37}$$

$$W_t^{\mathrm{q}} \varphi_t = q_t + q_{0t} \qquad \forall t, (\pi_{4t}) \tag{38}$$

where p_{0t} and q_{0t} denote the active and reactive power of ESS, respectively.

$$I_t y_t \le P_t^f \qquad \forall j \in J \ \forall t, (\pi_{5t}) \tag{39}$$

$$\|K_{nt} y_t\|_2 \le h_{nt}^T y_t \qquad \forall t, (\pi_{6nt}, \pi_{7nt}) \tag{40}$$

Formulas (34)–(40) can be transformed to Formulas (41)–(48) with dual theory.

$$\text{SP} : \sum_{t=1}^{T_{\max}} \max_{p_t, q_t, P_t^f, \pi_{1t}, \pi_{2t}, \pi_{3t}, \pi_{4t}, \pi_{5t}, \pi_{6nt}, \pi_{7nt}} \left(b_{1t}^T \pi_{1t} + b_{2t}^T \pi_{2t} + (p_t + p_{0t})^T \pi_{3t} + (q_t + q_{0t})^T \pi_{4t} + \left(P_t^f\right)^T \pi_{5t}\right) \tag{41}$$

$$\sum_{t=1}^{T_{\max}} \max_{p_t, q_t, P_t^f, \pi_{1t}, \pi_{2t}, \pi_{3t}, \pi_{4t}, \pi_{5t}, \pi_{6nt}, \pi_{7nt}} \left(b_{1t}^T \pi_{1t} + b_{2t}^T \pi_{2t} + (p_t + p_{0t})^T \pi_{3t} + (q_t + q_{0t})^T \pi_{4t} + \left(P_t^f\right)^T \pi_{5t}\right) \tag{42}$$

$$\text{s.t. } \|\pi_{6nt}\|_2 \le \pi_{7nt}, \forall t \tag{43}$$

$$R_t^T \pi_{1t} + M_t^T \pi_{2t} + \left(W_t^{\mathrm{P}}\right)^T \pi_{3t} + \left(W_t^{\mathrm{q}}\right)^T \pi_{4t} + I_t^T \pi_{5t} + \sum_n \left(K_{nt}^T \pi_{6nt} + h_{nt} \pi_{7nt}\right) = c_t, \forall t \tag{44}$$

$$\pi_{2t} \le 0, \forall t \tag{45}$$

$$p_t^{\min} \le p_t \le p_t^{\max}, \forall t \tag{46}$$

$$p_t^{\min} \circ \tan(\theta_{\mathrm{L}}) \le q_t \le p_t^{\max} \circ \tan(\theta_{\mathrm{L}}), \forall t \tag{47}$$

$$P_t^{f\min} \le P_t^f \le P_t^{f\max} \qquad \forall t \tag{48}$$

where π_t^1, π_t^2, π_t^3, π_{lt}^4, and π_{lt}^5 are the dual variables.

Let $\gamma_{t,n}^{\mathrm{P}} = \pi_{3t} \delta_{t,n}$, then the bilinear term $(p_t)^T \pi_{3t}$ in Equation (41) can be linearized as Equation (49) using the big-M method.

$$\begin{cases} (p_t)^T \pi_{3t} = \sum_n \left(p_{t,n}^{\min} \pi_{3t,n} + (p_{t,n}^{\max} - p_{t,n}^{\min}) \gamma_{t,n}^{\mathrm{P}}\right) \\ -M \delta_{t,n} \le \gamma_{t,n}^{\mathrm{P}} \le M \delta_{t,n} \\ -M(1 - \delta_{t,n}) \le \gamma_{t,n}^{\mathrm{P}} - \pi_{3t,n} \le M(1 - \delta_{t,n}) \\ \delta_{t,n} \in \{0,1\} \end{cases} \qquad \forall t, \forall n \tag{49}$$

where M is a big number.

Similarly, let $\gamma_{t,n}^{q} = \pi_{4t}\delta_{t,n}$, then the bilinear term $(q_t)^T \pi_{4t}$ in Equation (41) can be linearized as:

$$\begin{cases} (q_t)^T \pi_{4t} = \sum_n \left(p_{t,n}^{min} \tan(\theta_{L,n})\pi_{4t,n} + \left(p_{t,n}^{max} - p_{t,n}^{min} \right) \tan(\theta_{L,n})\gamma_{t,n}^{q} \right) \\ -M\delta_{t,n} \le \gamma_{t,n}^{q} \le M\delta_{t,n} \\ -M(1-\delta_{t,n}) \le \gamma_{t,n}^{q} - \pi_{4t,n} \le M(1-\delta_{t,n}) \end{cases} \quad \forall t, \forall n \quad (50)$$

Similarly, let $\gamma_{t,n}^{DG} = \lambda_t \pi_{5t,n}$. For the same kind of renewable DGs, such as a wind turbine, the bilinear term $\left(P_t^f \right)^T \pi_{5t}$ in Equation (41) can be linearized as:

$$\begin{cases} \left(P_t^f \right)^T \pi_{5t} = \sum_n \left(P_{t,n}^{fmin} \pi_{5t,n} + \left(P_{t,n}^{fmax} - P_{t,n}^{fmin} \right)\gamma_{t,n}^{DG} \right) \\ -M\lambda_t \le \gamma_{t,n}^{DG} \le M\lambda_t \\ -M(1-\lambda_t) \le \gamma_{t,n}^{DG} - \pi_{5t,n} \le M(1-\lambda_t) \\ \lambda_t \in \{0,1\} \end{cases} \quad \forall t, \forall n \quad (51)$$

3.3. Solution Steps

The flowchart of solving procedures is shown in Figure 2. The steps are as follows.
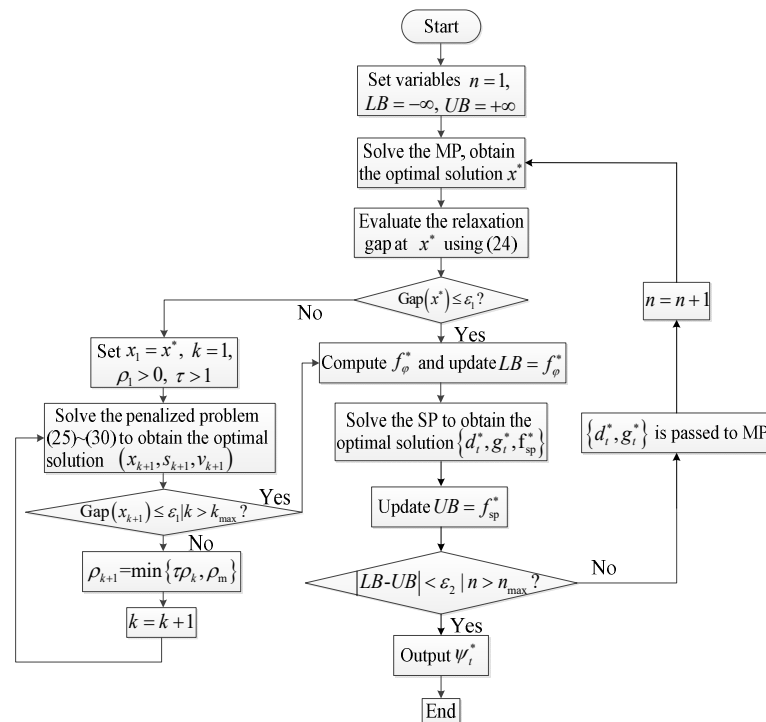
Figure 2. Flowchart of solving procedures.

P1: Set $LB = -\infty$, $UB = +\infty$, and $n = 1$.

P2: Solve MP to obtain the optimal solution x^*. Evaluate relaxation gaps at x^* as

$$\text{Gap}(x^*) = \max_t \max_{ij \in E} \left(l_{ij,t}^* u_{i,t}^* - \left(G_{ij,t}^* \right)^2 - \left(H_{ij,t}^* \right)^2 \right) \quad (52)$$

If $\text{Gap}(x^*) \le \varepsilon_1$, where ε_1 is a pre-specified tolerance, terminate and report the optimal solution x^*. Compute $f_\varphi^* = \sum_{t=1}^{T_{max}} \left(\sum_{(i,j) \in E} r_{ij} l_{ij,t} - \sum_{j \in J} P_{s,j,t} \right) \Delta t$ and update the lower bound to $LB = f_\varphi^*$. Jump to P6. If $\text{Gap}(x^*) > \varepsilon_1$, go to P3.

P3: Set an initial penalty coefficient $\rho_1 > 0$, a penalty growth rate parameter $\tau > 1$, and a penalty upper bound ρ_{m}. Let the iteration index $k = 1$, and the initial point $x_1 = x^*$.

P4: Form the linear approximation $\overline{g}_{ij}(x)$ at x_k $\overline{g}_{ij,t}(x, x_k) = g_{ij,t}(x_k) + \nabla g_{ij,t}(x_k)^T(x, x_k)$, $\forall (i, j) \in E, \forall t$ and solve the following penalized problem:

$$\min v(x, s) = f_{\mathrm{obj}}(x) + \rho_k \sum_{t=1}^{T_{\max}} \sum_{ij \in E} s_{ij,t} \tag{53}$$

$$s.t. x \in X, s_{ij,t} \geq 0, \forall (i, j) \in E, \forall t \tag{54}$$

$$f_{ij,t}(x) = \left(u_{i,t} + l_{ij,t} \right)^2 \tag{55}$$

$$g_{ij,t}(x) = \left(u_{i,t} - l_{ij,t} \right)^2 + 4 \left(G_{ij,t} \right)^2 + 4 \left(H_{ij,t} \right)^2 \tag{56}$$

$$f_{ij,t} - \overline{g}_{ij,t}(x, x_k) \leq s_{ij,t} \forall (i, j) \in E, \forall t \tag{57}$$

$$l_{ij,t} \leq \frac{\left(G^*_{ij,t,k-1} \right)^2 + \left(H^*_{ij,t,k-1} \right)^2}{u^*_{i,t,k-1}} \forall (i, j) \in E, \forall t \tag{58}$$

$$(2) \sim (18) \tag{59}$$

where $G^*_{ij,t,k-1}$, $H^*_{ij,t,k-1}$, and $u^*_{i,t,k-1}$ are the optimal active, reactive power and voltage magnitude square after $(k-1)^{\mathrm{th}}$ solving Equations (53)–(59). The optimal solution is (x_{k+1}, s_{k+1}), and the optimal objective function value is v_{k+1}.

P5: Evaluate the relaxation gap at x_{k+1}. If $\mathrm{Gap}(x_{k+1}) \leq \varepsilon_1$, terminate, and report $x^* = x_{k+1}$. Otherwise, update $\rho_{k+1} = \min\{\tau \rho_k, \rho_{\mathrm{m}}\}$, $k \leftarrow k + 1$. While $k < k_{\max}$, go to P2.

P6: Fix $\{\psi_t^*\}$ and solve the SP at each time period to obtain the worst scenario $\{d_t^*\}$, $\{g_t^*\}$. Compute the total optimal objective function $f_{\mathrm{sp}}^*(\psi_t^*)$ by accumulating that of each period.

P7: Update $UB = f_{\mathrm{sp}}^*(\psi_t^*)$. If $|LB - UB| < \varepsilon_2$ or $n > n_{\max}$ ($n_{\max}$ is the maximum number of iterations), terminate the program and output ψ_t^*. Otherwise, $\{d_t^*\}$ and $\{g_t^*\}$ are substituted into MP. Update $n \leftarrow n + 1$ and go to P2.

It is worth pointing out that system data are gathered a day in advance. Then, the program is performed. The settings are sent to and stored in each piece of adjustable equipment a day in advance. When communication errors occur within a day, the proposed method can be still applicable [27,28].

4. Numerical Analysis

In case 1, the 33-, 69-, and 123-bus systems are used to test the capabilities of the proposed method. The maximal active power of each PV plant and PMSG wind turbine is set to 100 and 200 kW, respectively. Since the penetration of DGs is low, the conic relaxations are exact. The computing rate of the two-stage multi-period mixed integer SOCP of the proposed method is compared with the CCG method.

In case 2, the 33-bus systems are used to test the capabilities of the proposed method. the active power of each PV plant is set to 1.5, 2.5, 3.5, 4.5, 5.5, and 6.5 MW. Since the penetration of DGs is very high, the conic relaxations are not exact. The computing and convergence rate of the single-period sequential SOCP of the proposed method is compared with [23,25,29].

In case 3, the 33-bus systems are used to test the capabilities of the proposed method. The maximal active power of each PV plant is set to 1.5 MW. Since the penetration of DGs is very high, the conic relaxations are not exact. The computing and convergence rate of two-stage multi-period mixed integer sequential SOCP using the proposed method is compared with [23,25,29].

In case 4, the 69- and 123-bus systems are used to test the capabilities of the proposed method. The maximal active power of each PV plant and PMSG wind turbine is set to 600

and 375 kW, respectively. Since the penetration of DGs is very high, the conic relaxations are not exact. The computing and convergence rate of two-stage multi-period mixed integer sequential SOCP using the proposed method is compared with the CCG method.

4.1. Case 1

The 33-, 69-, and 123-bus systems in [21] are used to test the capabilities of the proposed method. Some simulation conditions are set as follows. One PV plant is connected to bus 4–7, 14–17, 19, 20, 23, 26, 31, and 32 in the IEEE 33-bus system. Meanwhile, one PV plant is connected to buses 15, 19, 25–27, 33–35, 39, 41, 44, 48, 52–56, 58, and 67–69 in the PG69-bus system. The maximum active power and rated capacity of each PV plant is set to 100 kW and 100 kVA, respectively. The power factor angle range of each PV plant is set to be [−pi/2, pi/2]. The load and PV factor are shown in Figure 3. The convergence tolerances ε_1 and ε_2 are set to be 1.0×10^{-6} and 2.0×10^{-4}, respectively. The maximum iteration n_{max}, is set to be 5. K is set to 5. For the 33- and 69-bus systems, other simulation conditions are the same as [26].
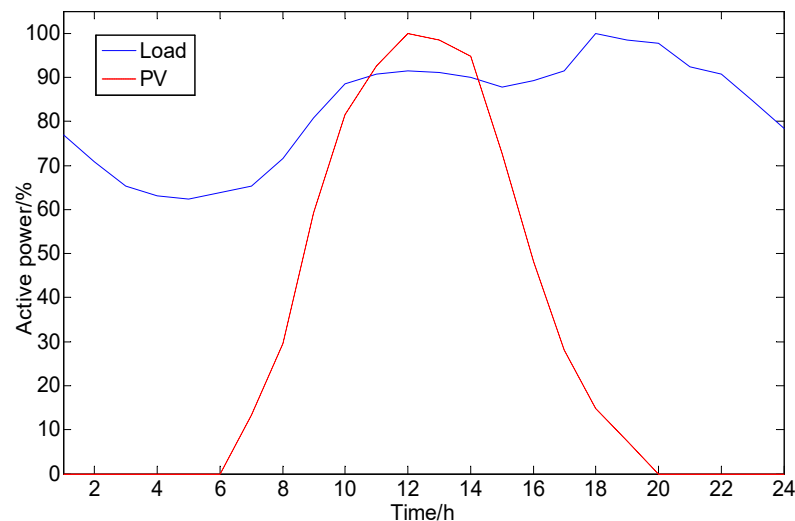
Figure 3. Load and PV factor in 24 h.

One permanent magnet synchronous generator (PMSG) wind turbine is connected to bus 33, 39, 48, 51, 56, 66, 70, 71, 75, 78, 85, 91, 96, 104, 106, 107, 114, 115, 118, and 122 in the IEEE 123-bus system. The maximum active power and capacity of each wind turbine is set to 200 kW and 200 kVA, respectively. The power factor angle range of each PMSG wind turbine is set to [−pi/2, pi/2]. The load and PMSG wind turbine factor is the same as [26]. One SCR is connected to bus 83, 88, 90, and 92. The capacities of the SCR are [−0.6, 0.6], [−0.15, 0.15], [−0.15, 0.15], and [−0.15, 0.15] MVar, while the step size is 0.1, 0.025, 0.025, and 0.025 MVar, respectively. One SVR is connected between bus 9 and 14, 25 and 26, 119 and 67, and 123 and 1, respectively. One ESS connected to bus 1 and 60, respectively. The charge and discharge efficiency of each ESS is 0.95. The capacity of ESS is 0.75 and 0.25 MWh, respectively. The maximum cycle of the ESS is set to be 3. Both the maximum charge and discharge power are 150 and 150 kW, respectively. One SVC is connected to node 114 and 116, respectively. The capacity of both SVCs is [−0.25, 0.25] MVar. The maximal current at each branch is set to 700 A. The voltage magnitude bound of each node is set to [0.9, 1.1] p.u. The base power of the systems is set as 5 MVA. The base voltage of the systems is chosen to be 4.16 kV. K is set to 5. The convergence tolerance ε_1 and ε_2 are set to be 1.0×10^{-6} and 5.0×10^{-4}, respectively. The maximum iteration n_{max} is set to be 10. The tolerances of relative gaps are properly chosen such that the programs can run fluently. For fairness of comparison, they are set the same for the proposed and CCG methods. The simulation result is a global optimum. This is because the mixed integer second-order cone programming software package of MOSEK is used to solve the problem.

The objective function values of the master- and sub-problem, iterations, and computational time for the 33- and 69-bus systems are shown in Tables 1–4. As can be seen, the objective function values of the proposed method fit that of the improved CCG method (the sub-problem is solved with the proposed method) very close for different —that is, the precision of the proposed method is high enough. However, the average number of iterations and computational time of the proposed method are less than those of the improved CCG method.

Table 1. Objective function values for the 33-bus network.

| ζ | Objective Function Values (p.u.) | | | |
| | Improved CCG | | Proposed Method | |
	MP	**SP**	**MP**	**SP**
0.1	−0.0933	−0.0934	−0.0934	−0.0934
0.2	0.0072	0.0072	0.0072	0.0072
0.3	0.1194	0.1194	0.1184	0.1184
0.4	0.2408	0.2409	0.2408	0.2409
0.5	0.3754	0.3755	0.3754	0.3755
0.6	0.5231	0.5232	0.5231	0.5232

Table 2. Iterations and computational time for the 33-bus network.

| ζ | Improved CCG | | Proposed Method | |
	Iterations	**Time (s)**	**Iterations**	**Time (s)**
0.1	3	46.155	2	35.662
0.2	2	33.772	2	36.256
0.3	5	100.713	2	33.577
0.4	2	19.926	2	35.015
0.5	2	19.734	2	33.844
0.6	2	21.128	2	28.190

Table 3. Objective function values for the 69-bus network.

| ζ | Objective Function Values (p.u.) | | | |
| | Improved CCG | | Proposed Method | |
	MP	**SP**	**MP**	**SP**
0.1	−0.0660	−0.0661	−0.0660	−0.0661
0.2	0.0270	0.0269	0.0269	0.0267
0.3	0.1464	0.1462	0.1440	0.1439
0.4	0.2694	0.2692	0.2656	0.2654
0.5	0.4080	0.4072	0.4016	0.4014
0.6	0.5561	0.5544	0.5502	0.5501

Table 4. Iterations and computational time for the 69-bus network.

| ζ | Improved CCG | | Proposed Method | |
	Iterations	**Time (s)**	**Iterations**	**Time (s)**
0.1	2	65.025	2	77.585
0.2	2	75.127	2	82.130
0.3	3	110.968	2	69.863
0.4	3	113.343	2	69.791
0.5	5	264.499	4	139.552
0.6	5	272.656	3	111.973

In Table 4, when the forecast errors ζ are 0.1 and 0.2, the computing time of the method proposed is a litter longer than the improved CCG. It is correct. This is because both methods converge with two iterations. Since the scale of the problem is not very large, the computing time of the method proposed could be a litter longer than the improved CCG because of numerical stability.

The active power of all the ESS is zero. This is because reactive power is more efficient than active power to reduce network losses. The injected reactive power of ESS at node 16 when ζ is 0.2 for the 33-bus system is shown in Figure 4. It can be seen that when the load is high (low), the injected reactive power of ESS at node 16 is also high (low). Specifically, when the load is minimal at time period 5, the injected reactive power of ESS at node 16 is also minimal. Contrastingly, when the load is at its peak during time periods 11–13 and 17–22, the injected reactive power of ESS at node 16 also reaches its maximum. This is because, when the load is high (low), the reactive power demand is high (low). Therefore, a large (small) amount of reactive power is produced by the ESS at node 16 to reduce the active power losses of network.
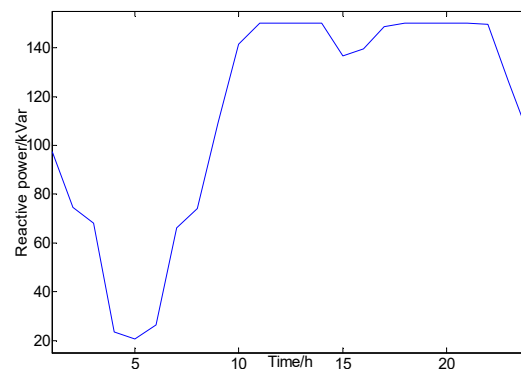
Figure 4. Reactive power injection from EES at node 16 for the 33-bus system.

The objective function values of the master- and sub-problem, iterations, and computational time for the 123-bus system are shown in Tables 5 and 6, respectively. As can be seen, the gaps of the objective function values between the master and sub-problem of the proposed method for each ζ are much less than those of the improved CCG and CCG method. Moreover, the iterations and computational time of the proposed method for each ζ are much less than those of the improved CCG and CCG method. This is because, increases to variables and constraints are not needed to solve the master problem using the proposed method and the solving complexity of the sub-problem is much less than CCG method.

Table 5. Objective function values for the 123-bus network.

| ζ | Objective Function Values (p.u.) | | | | | |
| | Improved CCG | | CCG | | Proposed Method | |
	MP	SP	MP	SP	MP	SP
0.1	−2.0870	−2.0466	−2.1100	−2.0377	−2.0633	−2.0634
0.2	−2.0613	−2.0277	−2.0645	−2.0213	−2.0403	−2.0403
0.3	−2.0101	−2.0061	−2.0135	−1.9599	−2.0159	−2.0164
0.4	−1.9388	−1.9072	−1.9418	−1.8868	−1.9240	−1.9240
0.5	−1.8582	−1.8268	−1.8617	−1.8068	−1.8447	−1.8450
0.6	−1.7764	−1.7321	−1.7752	−1.7144	−1.7568	−1.7573

Table 6. Iterations and computational time for the 123-bus network.

ζ	Improved CCG		CCG		Proposed Method	
	Iterations	**Time (s)**	**Iterations**	**Time (s)**	**Iterations**	**Time (s)**
0.1	10	3524.916	10	3810	2	183.664
0.2	10	3152.919	10	4248	2	195.945
0.3	10	3318.348	10	4258	2	193.753
0.4	10	3151.459	10	4606	2	192.636
0.5	10	3091.671	10	4017	2	192.460
0.6	10	3010.364	10	4154	3	299.966

The maximum gaps of conic relaxation under different ζ of the three systems are shown in Table 7. As can be seen, they are all less than 1.0×10^{-6}, which indicates that the conic relaxations are exact. This is because the penetration rate of DGs is very low.

Table 7. Maximum gaps of conic relaxation.

ζ	33-Bus System	69-Bus System	123-Bus System
0.1	6.3948×10^{-9}	7.9871×10^{-7}	6.4669×10^{-8}
0.2	8.8074×10^{-9}	3.6889×10^{-8}	5.0020×10^{-9}
0.3	7.8910×10^{-9}	4.1979×10^{-8}	1.3896×10^{-8}
0.4	8.4152×10^{-9}	5.3522×10^{-8}	3.1927×10^{-8}
0.5	9.4049×10^{-9}	8.7201×10^{-7}	7.4779×10^{-8}
0.6	8.0618×10^{-9}	7.3739×10^{-7}	7.8610×10^{-8}

The optimal selection of DGs providing ancillary services for the three systems when ζ is 0.2 is shown in Tables 8–10. It can be seen that PV plants at nodes 26, 31, and 32 in the 33-bus system, as well as those at nodes 44, 48, and 52 in the 69-bus system, have always been selected to provide ancillary services. For the 123-bus system, during time periods 1–9 when the power generation of DGs is high, PMSG wind turbines at nodes 71, 104, 107, 114 are always selected to provide ancillary services. Contrastingly, during time periods 10–24 when wind power generation is low, PMSG wind turbines at nodes 48, 56, 66, and 122 are always selected to provide ancillary services.

Table 8. Optimal selection of PV plants providing ancillary services in the 33-bus network.

Time	PV Bus Number	Time	PV Bus Number	Time	PV Bus Number
1	7, 23, 26, 31, 32	9	7, 23, 26, 31, 32	17	7, 23, 26, 31, 32
2	7, 23, 26, 31, 32	10	7, 23, 26, 31, 32	18	6, 7, 26, 31, 32
3	20, 23, 26, 31, 32	11	7, 23, 26, 31, 32	19	6, 7, 26, 31, 32
4	14, 20, 26, 31, 32	12	7, 23, 26, 31, 32	20	6, 7, 26, 31, 32
5	14, 20, 26, 31, 32	13	7, 23, 26, 31, 32	21	7, 23, 26, 31, 32
6	14, 20, 26, 31, 32	14	7, 23, 26, 31, 32	22	7, 23, 26, 31, 32
7	20, 23, 26, 31, 32	15	7, 23, 26, 31, 32	23	7, 23, 26, 31, 32
8	7, 23, 26, 31, 32	16	7, 23, 26, 31, 32	24	7, 23, 26, 31, 32

Table 9. Optimal selection of PV plants providing ancillary services in 69-bus network.

Time	PV Bus Number	Time	PV Bus Number	Time	PV Bus Number
1	39, 44, 48, 52, 54	9	39, 44, 48, 52, 53	17	44, 48, 52, 53, 54
2	25, 39, 44, 48, 52	10	44, 48, 52, 53, 54	18	44, 48, 52, 53, 54
3	25, 39, 44, 48, 52	11	44, 48, 52, 53, 54	19	44, 48, 52, 53, 54
4	25, 39, 44, 48, 52	12	44, 48, 52, 53, 54	20	44, 48, 52, 53, 54
5	15, 39, 44, 48, 52	13	44, 48, 52, 53, 54	21	39, 48, 52, 53, 54
6	25, 39, 44, 48, 52	14	44, 48, 52, 53, 54	22	39, 48, 52, 53, 54
7	25, 39, 44, 48, 52	15	44, 48, 52, 53, 54	23	39, 48, 52, 53, 54
8	25, 39, 44, 48, 52	16	44, 48, 52, 53, 54	24	44, 48, 52, 53, 54

Table 10. Optimal selection of wind turbines providing ancillary services in the 123-bus network.

Time	WT Bus Number	Time	WT Bus Number	Time	WT Bus Number
1	71, 85, 104, 107, 114	9	70, 71, 104, 107, 114	17	33, 48, 56, 66, 122
2	70, 71, 104, 107, 114	10	48, 56, 66, 78, 122	18	39, 48, 56, 66, 122
3	71, 85, 104, 107, 114	11	33, 48, 56, 66, 122	19	39, 48, 56, 66, 122
4	71, 85, 104, 107, 114	12	33, 48, 56, 66, 122	20	39, 48, 56, 66, 122
5	71, 85, 104, 107, 114	13	33, 48, 56, 66, 122	21	39, 48, 56, 66, 122
6	71, 85, 104, 107, 114	14	48, 56, 66, 78, 122	22	39, 48, 56, 66, 122
7	70, 71, 104, 107, 114	15	33, 48, 56, 66, 122	23	48, 56, 66, 78, 122
8	70, 71, 104, 107, 114	16	33, 48, 56, 66, 122	24	48, 56, 66, 78, 122

The injected reactive power of ESS at node 1 when ζ is 0.2 for the 123-bus system is shown in Figure 5. It can be seen that when load minus the power generation of a wind turbine is high (low), the injected reactive power of ESS at node 16 is also high (low). Since the location of ESS is near to the root node, when the forward power flow is high, the ESS must inject a lot of reactive power to raise the voltage. Contrastingly, when the reverse power flow is high, the ESS must absorb a lot of reactive power to lower the voltage.
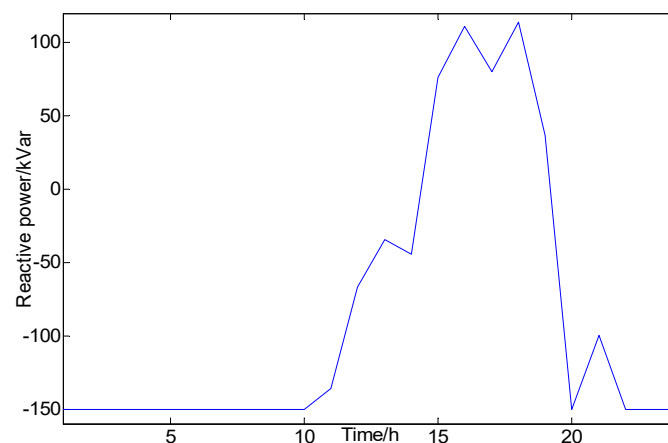
Figure 5. Reactive power injection from EES at node 1 for the 123-bus system.

4.2. Case 2

In the 33-bus system, the active power of each PV plant is set very high to test the capability of the proposed method. The active power of each PV plant is set to 1.5 MW, and the power factor is set to 1. All the PV plants provide ancillary services. There is not any ESS, SCR, SVR, or SVC in the system. Therefore, a single time period model is formulated. The tolerance ε_1 is set to be 1.0×10^{-6}. The maximum number of iterations $k_{\max}$ is set to be 30. The logarithms of the maximum gaps of conic relaxation for solving the deterministic master problem with different methods are shown in Figure 6a–d. As can be seen, the program using the proposed method converges within 5 iterations, while

it takes 14 iterations to converge using the method in [25]. Further, it does not converge using the method in [23,29].
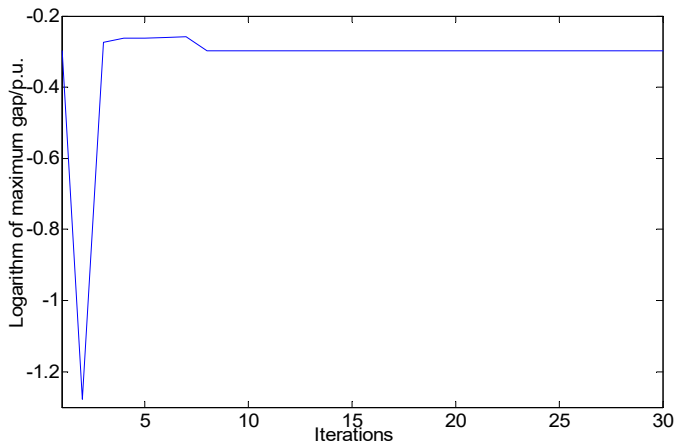
(**a**) Using the method in [29].
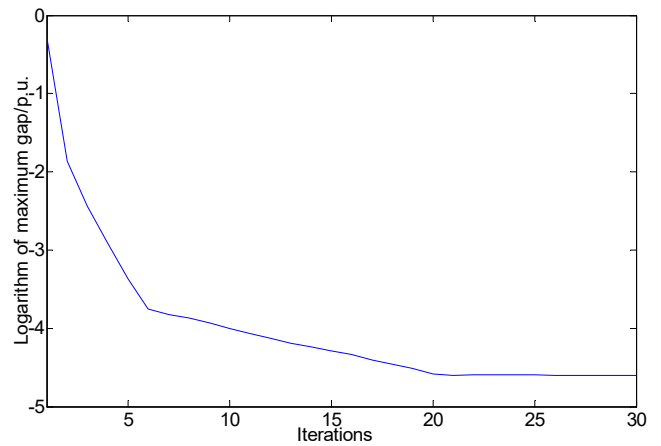
(**b**) Using the method in [23].
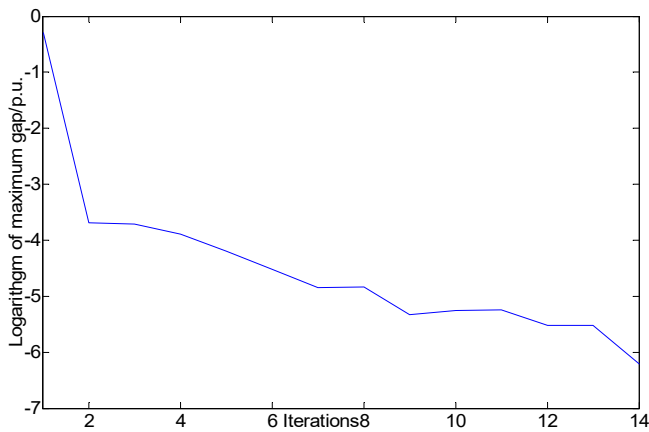
(**c**) Using the method in [25].
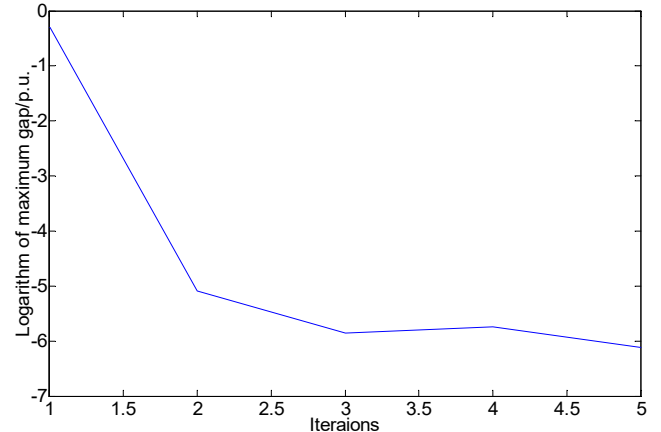
(**d**) Using the proposed method.
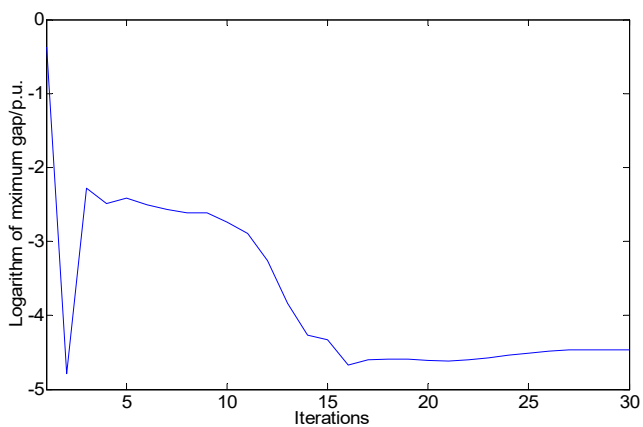
(**e**) Using the method in [25].
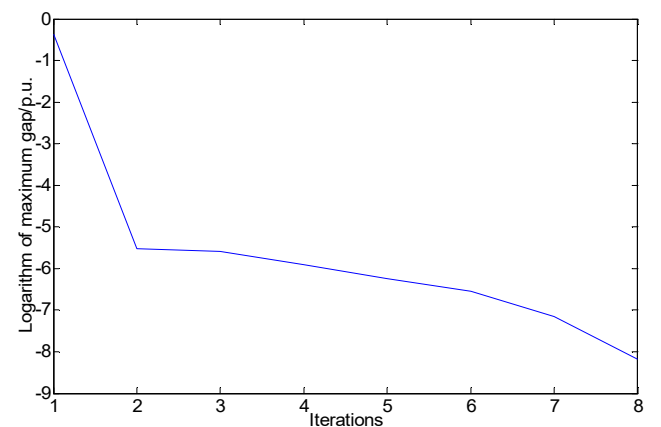
(**f**) Using the proposed method.

Figure 6. Comparisons on maximum gaps of conic relaxation.

Set the output active power and rated capacity of each PV plant to 2.5 MW and 2.5 MVA, respectively, and the tolerance ε_1 to 1.0×10^{-8}. The logarithms of the maximum gaps of conic relaxation for solving the deterministic master problem with the method

in [25] and the proposed method are shown in Figure 6e,f. As can be seen, the program does not converge after 30 iterations using the method in [25]. Nevertheless, it only takes eight iterations to converge using the proposed method.

Set the tolerance ε_1 to 1.0×10^{-6}, power factor to 1 and maximal iterations to 30. The number of iterations after solving the deterministic master problem under different active powers of PV plants is shown in Table 11. As can be seen, the program using the proposed method converges within five iterations under all the situations, which is much less than other methods.

Table 11. Number of iterations with different methods.

Active Power of Each PV (MW)	Proposed Method	Method in [23]	Method in [25]	Method in [29]
1.5	5	30	14	30
2.5	5	30	30	30
3.5	4	30	30	30
4.5	5	30	30	30
5.5	4	30	30	30
6.5	4	30	30	30

4.3. Case 3

Set the maximal active power and rated capacity of each PV plant to 1.5 MW and 1.5 MVA, respectively, in the 33-bus system. The objective function values of the master- and sub-problem, iterations, and computational time for the 33-bus system when ζ is 0.2 are shown in Tables 12–15. As can be seen, the objective function values of the master and sub-problem using the proposed method and that of [25] agree very well for each ζ. However, the number of iterations and computational time of the proposed method are much less than the method in [25]. Further, the method in [23,29] fails since the master problem is infeasible except when ζ is 0.1 using the method in [23].

Table 12. Objective function values.

ζ	Objective Function (p.u.)			
	Method in [25]		Proposed Method	
	MP	SP	MP	SP
0.1	−0.7654	−0.7654	−0.7655	−0.7655
0.2	−0.7323	−0.7323	−0.7323	−0.7323
0.3	−0.6992	−0.6992	−0.6992	−0.6992
0.4	−0.6660	−0.6660	−0.6660	−0.6660
0.5	−0.6329	−0.6329	−0.6329	−0.6329
0.6	−0.5997	−0.5997	−0.5997	−0.5997

Table 13. Iterations and computational time.

ζ	Method in [25]		Proposed Method	
	Iterations	Time (s)	Iterations	Time (s)
0.1	2	31.433	2	13.896
0.2	2	31.894	2	15.148
0.3	2	31.938	2	11.402
0.4	2	29.879	2	13.179
0.5	2	31.046	2	11.724
0.6	2	33.076	2	11.168

Table 14. Objective function values.

| ζ | Objective Function Values (p.u.) | | | |
| | Method in [23] | | Method in [29] | |
	MP	SP	MP	SP
0.1	−0.7619	−0.7655	Infeasible	−0.7655
0.2	Infeasible	58.4681	Infeasible	−0.7323
0.3	Infeasible	60.6725	Infeasible	−0.6992
0.4	Infeasible	62.8792	Infeasible	−0.6660
0.5	Infeasible	65.0870	Infeasible	−0.6329
0.6	Infeasible	67.2952	Infeasible	−0.5997

Table 15. Iterations and computational time.

| ζ | Method in [23] | | Method in [29] | |
	Iterations	Time (s)	Iterations	Time (s)
0.1	5	46.240	2	57.417
0.2	5	20.606	2	56.451
0.3	5	23.765	2	53.611
0.4	5	22.276	2	56.217
0.5	5	20.324	2	56.976
0.6	5	20.741	2	56.599

4.4. Case 4

Set the maximal active power and rated capacity of each PV plant to 600 kW and 600 kVA, respectively. Moreover, set the maximal active power and rated capacity of each PMSG wind turbine to 375 kW and 375 kVA, respectively. Further, set the tolerance ε_2 to 0.0005 for the 69-bus system and 0.003 for the 123-bus system. Other simulation conditions are the same as case 1. The maximal gaps of conic relaxations of both systems are always less than 1.0×10^{-6} for the sub-problem. However, they are a little less than 1.0 but far larger than 1.0×10^{-6} for the first iterations after solving the master problem. To this end, the CCP is applied, and a sequential SOCP is solved. The objective function values of the proposed method when ζ is 0.5 are shown in Table 16. The iterations and computational time are shown in Table 17. It can be seen that the program converges with three iterations with the proposed method for both systems. The computing rate is also acceptable for both systems, although it is slower than case 1. Further, when the methods in [23,29] are adopted, the programs do not converge.

Table 16. Objective function values for the 69- and 123-bus systems.

| ζ | Objective Function Values (p.u.) | | | |
| | 69-Bus System | | 123-Bus System | |
	MP	SP	MP	SP
0.5	−1.2676	−1.2679	−3.7354	−3.7379

Table 17. Iterations and computational time for the 69- and 123-bus systems.

| ζ | 69-Bus System | | 123-Bus System | |
	Iterations	Time (s)	Iterations	Time (s)
0.5	3	495.609	3	1985.721

The logarithm values of maximal gaps of conic relaxation for the master problem of the 69-bus system at the third iterations between the master and sub-problem using the

proposed method is shown in Figure 7. It can be seen that it just needs two iterations for the sequential SOCP to converge. Further, the logarithm values of the maximal gaps of conic relaxation for the master problem of the 123-bus system at the third iterations between the master and sub-problem using the proposed method are shown in Figure 8. It can be seen that it just needs four iterations for the sequential SOCP to converge. Therefore, the efficiency of the proposed method is high.
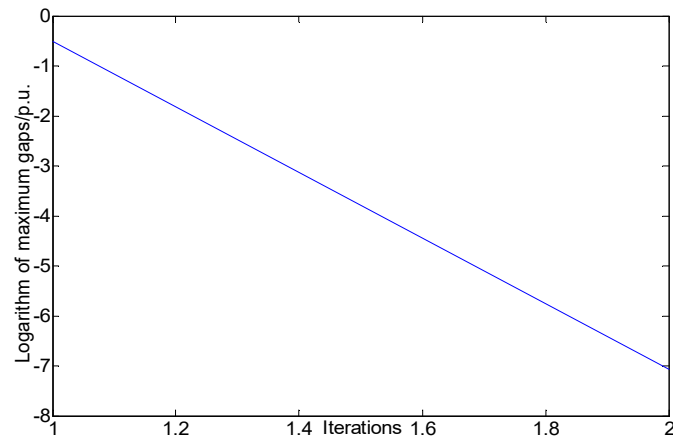
Figure 7. Logarithms of maximal gaps of conic relaxation when the rated capacity of each PV plant is 600 kVA for the 69-bus system.
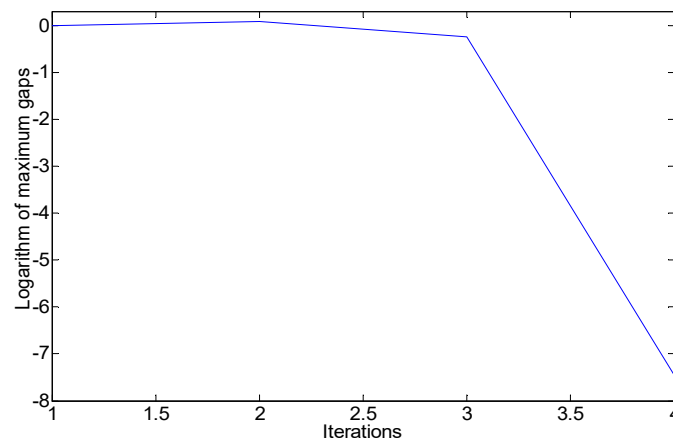
Figure 8. Logarithms of maximum gaps of conic relaxation when the rated capacity of each wind turbine is 375 kVA for the 123-bus system.

The optimal selection of PV plants providing ancillary services in the 69-bus systems is shown in Table 18. It can be seen that PV plants at nodes 15, 19, and 25–27 have always been selected to provide ancillary services during time periods 10–14 when the solar power generation is high since they are furthest from the root node. Moreover, PV plants at nodes 39 and 52 have always been selected to provide ancillary services when the solar power generation is low.

Table 18. Optimal selection of PV plants providing ancillary services in the 69-bus network.

Time	PV Bus Number	Time	PV Bus Number	Time	PV Bus Number
1	15, 39, 44, 48, 52	9	15, 26, 27, 39, 52	17	39, 44, 48, 52, 53
2	15, 39, 44, 48, 52	10	15, 19, 25, 26, 27	18	15, 39, 44, 48, 52
3	15, 39, 44, 48, 52	11	15, 19, 25, 26, 27	19	33, 39, 44, 48, 52
4	15, 39, 44, 48, 52	12	15, 19, 25, 26, 27	20	33, 39, 44, 48, 52
5	15, 39, 44, 48, 52	13	15, 19, 25, 26, 27	21	15, 39, 44, 48, 52
6	15, 39, 44, 48, 52	14	15, 19, 25, 26, 27	22	15, 39, 44, 48, 52
7	15, 39, 44, 48, 52	15	19, 25, 26, 27, 39	23	15, 39, 44, 48, 52
8	39, 48, 52, 53, 54	16	15, 27, 39, 48, 52	24	15, 39, 44, 48, 52

The reactive power injections and active power curtailment of DGs for the 69-bus system are shown in Table 19. It can be seen that, when the power generation of PV plants is high during time periods 9–15, a large amount of reactive power is absorbed and active power is cut down to keep the voltage lower than 1.1 p.u. and current lower than 400 A. Further, when the power generation of PV plant is zero at night, a large amount of reactive power are injected to reduce power losses of lines.

Table 19. Optimal reactive power injection of PV plants in the 69-bus network.

Time	Reactive Power (kvar)	Time	Reactive Power (kvar)
1	175, 588, 128, 232, 590	13	−106, −172, −426, −480, −508
2	151, 540, 108, 211, 489	14	−106, −173, −430, −484, −512
3	130, 498, 92, 192, 401	15	−181, −442, −495, −522, 19
4	120, 480, 85, 184, 363	16	88, −406, −415, 175, 415
5	117, 474, 83, 182, 350	17	253, −240, 491, 544, -8.9×10^{-4}
6	124, 400, 87, 187, 376	18	263, 598, 51, 598, 598
7	95, 496, 61, 180, 369	19	43, 600, 32, 600, 600
8	−513, 252, 537, −268, 45	20	71, 600, 57, 600, 600
9	−275, −393, −415, 29, −275	21	237, 600, −29, 531, 600
10	−107, −175, −435, −489, −517	22	230, 600, −35, 500, 600
11	−106, −172, −427, −481, −509	23	206, 600, −58, 376, 600
12	−105, −171, −425, −478, −507	24	182, 599, −80, 253, 600

The minimum and maximum voltages and maximum currents for the 69- and 123-bus systems are shown in Figures 9–12, respectively. It can be seen that, although the penetration of DGs is very high and the uncertainty of load and power generation of DGs is large, the currents and voltages are still within the rated range, even for the worst scenario using the proposed method.
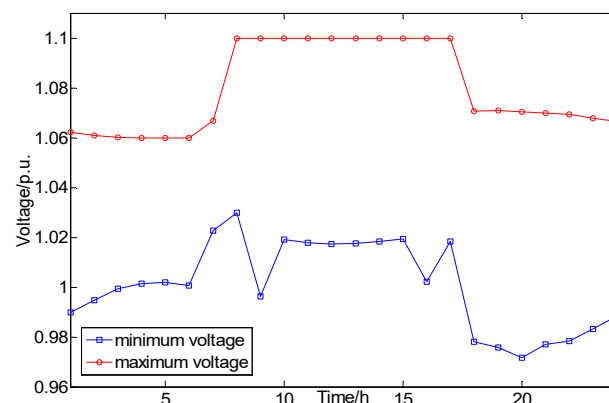
Figure 9. Minimum and maximum voltages in the 69-bus system.
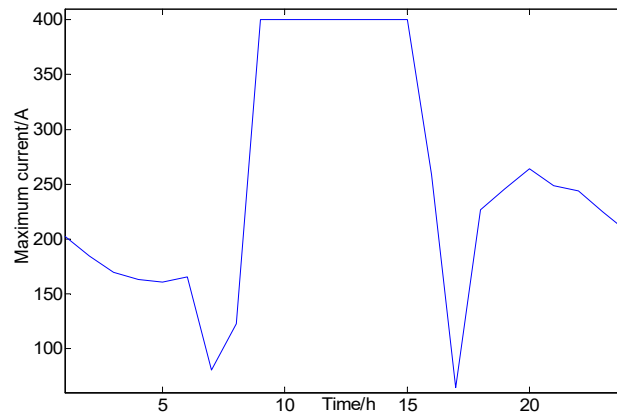
Figure 10. Maximum currents in the 69-bus system.
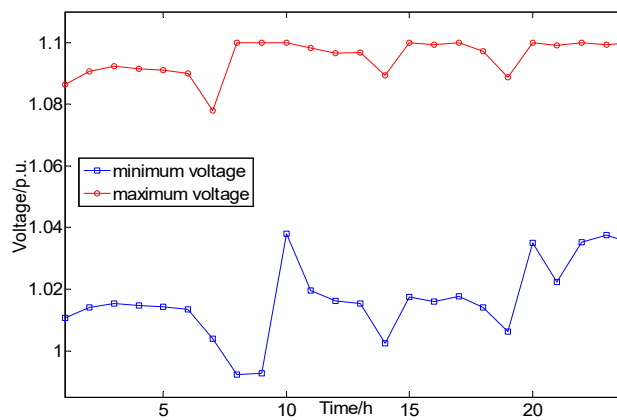
Figure 11. Minimum and maximum voltages for the 123-bus system.
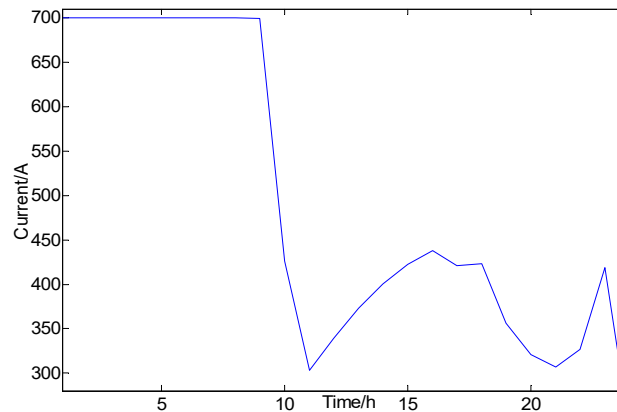
Figure 12. Maximum currents in the 123-bus system.

5. Conclusions

In this paper, considering SVR, SCR, SVC, and ESS, a two-stage multi-period SOCP robust optimization model with partial DGs providing ancillary services is developed. The active power losses of ESS are included in the objective function and its reactive power is utilized. Then, a method that direct iteratively solves the first- and second-stage model without increasing any variables and constraints in the master problem is presented. Moreover, it is only needed to solve each single period model of the second-stage problem. As a result, with much less storage capacity, the computational rate of the proposed method is greatly enhanced. Specifically, the simulation results of the IEEE 123-bus system indicate that the computing rate of the proposed method is about 12–22 times higher than the CCG method.

If the conic relaxation is not exact, a sequential SOCP is formulated in which the concave terms are approximated by linear functions and updated at each iteration with a linear inequality of each line. As an outcome, the computing rate is greatly enhanced and the global optimal solution can be recovered.

Author Contributions: Conceptualization, J.Z.; methodology, M.C.; software, J.Z.; validation, J.Z.; formal analysis, J.Z.; investigation, J.Z.; resources, Y.H.; data curation, M.C.; writing—original draft preparation, J.Z.; writing—review and editing, M.C.; visualization, M.C.; supervision, Y.H.; project administration, Y.H.; funding acquisition, Y.H. All authors have read and agreed to the published version of the manuscript.

Conflicts of Interest: The authors declare no conflict of interest.

References

1. Zhang, J.; Cui, M.; Li, B.; Fang, H.; He, Y. Fast solving method based on linearized equations of branch power flow for coordinated charging of EVs (EVCC). *IEEE Trans. Veh. Technol.* **2019**, *68*, 4404–4418. [CrossRef]
2. Farivar, M.; Clarke, C.R.; Low, S.H.; Chandy, K.M. Inverter VAR control for distribution systems with renewable. In Proceedings of the IEEE International Conference on Smart Grid Communications, Brussels, Belgium, 17–20 October 2011; pp. 457–462. [CrossRef]
3. Dommel, H.W.; Tinney, W.F. Optimal power flow solutions. *IEEE Trans. Power Appar. Syst.* **1968**, *87*, 1866–1876. [CrossRef]
4. Baran, M.E.; Wu, F.F. Optimal capacitor placement on radial distribution systems. *IEEE Trans. Power Deliv.* **1989**, *4*, 725–734. [CrossRef]
5. Baran, M.; Wu, F. Optimal sizing of capacitors placed on a radial distribution system. *IEEE Trans. Power Deliv.* **1989**, *4*, 735–743. [CrossRef]
6. Lavaei, J.; Low, S.H. Zero duality gap in optimal power flow problem. *IEEE Trans. Power Syst.* **2012**, *27*, 92–107. [CrossRef]
7. Zhang, B.; Tse, D. Geometry of injection regions of power networks. *IEEE Trans. Power Syst.* **2013**, *28*, 788–797. [CrossRef]
8. Lavaei, J.; Tse, D.; Zhang, B. Geometry of power flows and optimization in distribution networks. *IEEE Trans. Power Syst.* **2014**, *29*, 572–583. [CrossRef]
9. Farivar, M.; Low, S.H. Branch flow model: Relaxations and convexification-Part I. *IEEE Trans. Power Syst.* **2013**, *28*, 2554–2564. [CrossRef]
10. Farivar, M.; Low, S.H. Branch flow model: Relaxations and convexification-Part II. *IEEE Trans. Power Syst.* **2013**, *28*, 2565–2572. [CrossRef]
11. Li, N.; Chen, L.; Low, S.H. Exact convex relaxation of OPF for radial networks using branch flow model. In Proceedings of the IEEE 3rd International Conference on Smart Grid Communications, Tainan, Taiwan, 5–8 November 2012; pp. 7–12. [CrossRef]
12. Huang, S.; Wu, Q.; Wang, J.; Zhao, H. A sufficient condition on convex relaxation of AC optimal power flow in distribution networks. *IEEE Trans. Power Syst.* **2017**, *32*, 1359–1368. [CrossRef]
13. Gan, L.; Li, N.; Topcu, U.; Low, S.H. Exact convex relaxation of optimal power flow in radial networks. *IEEE Trans. Autom. Control* **2015**, *60*, 72–87. [CrossRef]
14. Nick, M.; Cherkaoui, R.; Le Boudec, J.-Y.; Paolone, M. An exact convex formulation of the optimal power flow in radial distribution networks including transverse components. *IEEE Trans. Autom. Control* **2018**, *63*, 682–697. [CrossRef]
15. Nguyen, Q.H.; Padullaparti, H.V.; Lao, K.-W.; Santoso, S.; Ke, X.; Samaan, N.A. Exact optimal power dispatch in unbalanced distribution systems with high PV penetration. *IEEE Trans. Power Syst.* **2019**, *34*, 718–728. [CrossRef]
16. Robbins, B.A.; Zhu, H.; Dominguez-Garcia, A.D. Optimal tap setting of voltage regulation transformers in unbalanced distribution systems. *IEEE Trans. Power Syst.* **2016**, *31*, 256–267. [CrossRef]
17. Dall'Anese, E.; Zhu, H.; Giannakis, G. Distributed optimal power flow for smart microgrids. *IEEE Trans. Smart Grid* **2013**, *4*, 1464–1475. [CrossRef]
18. Zafar, R.; Ravishankar, J.; Fletcher, J.E.; Pota, H.R. Optimal Dispatch of Battery Energy Storage System Using Convex Relaxations in Unbalanced Distribution Grids. *IEEE Trans. Ind. Inform.* **2020**, *16*, 97–108. [CrossRef]
19. Xiang, Y.; Liu, J.; Liu, Y. Robust energy management of microgrid with uncertain renewable generation and load. *IEEE Trans. Smart Grid* **2016**, *7*, 1034–1043. [CrossRef]

20. Lee, C.; Liu, C.; Mehrotra, S.; Bie, Z. Robust distribution network reconfiguration. *IEEE Trans. Smart Grid* **2015**, *6*, 836–842. [CrossRef]

21. Ding, T.; Liu, S.; Yuan, W.; Bie, Z.; Zeng, B. A two-stage robust reactive power optimization considering uncertain wind power integration in active distribution networks. *IEEE Trans. Sustain. Energy* **2016**, *7*, 301–311. [CrossRef]

22. Zeng, B.; Zhao, L. Solving two-stage robust optimization problems using a column-and-constraints generation method. *Oper. Res. Lett.* **2013**, *41*, 457–461. [CrossRef]

23. Gao, H.; Liu, J.; Wang, L. Robust coordinated optimization of active and reactive power in active distribution systems. *IEEE Trans. Smart Grid* **2017**, *9*, 4436–4447. [CrossRef]

24. Ding, T.; Li, C.; Yang, Y.; Jiang, J.; Bie, Z.; Blaabjerg, F. A two-stage robust optimization for centralized-optimal dispatch of photovoltaic inverters in active distribution networks. *IEEE Trans. Sustain. Energy* **2017**, *8*, 744–754. [CrossRef]

25. Wei, W.; Wang, J.; Li, N.; Mei, S. Optimal Power Flow of Radial Networks and Its Variations: A Sequential Convex Optimization Approach. *IEEE Trans. Smart Grid* **2017**, *8*, 2974–2987. [CrossRef]

26. Zhang, J.; Cui, M.; He, Y.; Li, F. Multi-period fast robust optimization of active and reactive power in active distribution networks. *TechRxiv* **2020**. [CrossRef]

27. Cui, M.; Wang, J. Deeply hidden moving-target-defense for cybersecure unbalanced distribution systems considering voltage stability. *IEEE Trans. Power Syst.* **2021**, *36*, 1961–1972. [CrossRef]

28. Chunyu, C.; Mingjian, C.; Xin, F.; Bixing, R.; Yang, C. Load altering attack-tolerant defense strategy for secondary frequency control system. *Appl. Energy* **2020**, *280*, 116015. [CrossRef]

29. Abdelouadoud, S.; Girard, R.; Neirac, F.; Guiot, T. Optimal power flow of a distribution system based on increasingly tight cutting planes added to a second order cone relaxation. *Int. J. Electr. Power Energy Syst.* **2015**, *69*, 9–17. [CrossRef]